This article has been accepted for publication in a future issue of this journal, but has not been fully edited. Content may change prior to final publication. Citation information: DOI 10.1109/TNS.2016.2644663, IEEE Transactions on Nuclear Science

First Principles Modeling of RFQ Cooling System and Resonant Frequency Responses for Fermilab's PIP-II Injector Test

J. P. Edelen, *Member, IEEE,* A. L. Edelen, *Student Member, IEEE,* D. Bowring, *Member, IEEE*, B. E. Chase, J. Steimel, S. G. Biedron, *Senior Member, IEEE,* S. V. Milton, *Fellow, IEEE*

***Abstract*—In this paper we develop an a priori method for simulating dynamic resonant frequency and temperature responses in a radio frequency quadrupole (RFQ) and its associated water-based cooling system respectively. Our model provides a computationally efficient means to evaluate the transient response of the RFQ over a large range of system parameters. The model was constructed prior to the delivery of the PIP-II Injector Test RFQ and was used to aid in the design of the water-based cooling system, data acquisition system, and resonance control system. Now that the model has been validated with experimental data, it can confidently be used to aid in the design of future RFQ resonance controllers and their associated water-based cooling systems. Without any empirical fitting, it has demonstrated the ability to predict absolute temperature and frequency changes to 11% accuracy on average, and relative changes to 7% accuracy.**

I. Introduction

In ion accelerators, radio frequency quadrupoles (RFQs) are used to provide both acceleration and strong focusing of the beam, typically for injection into subsequent acceleration stages. In order to ensure proper acceleration and focusing in the RFQ, low-level RF (LLRF) control is used to maintain the field amplitude and phase. In the presence of detuning this is accomplished in part by increasing the forward power, thus taking advantage of the available power overhead in the RF amplifiers. However, the cost of additional power overhead scales with the power of the amplifier. At the power requirements for most RFQs, it is more cost effective to design and implement RF and water systems that facilitate precise control of the RFQ's resonant frequency. A model that fully characterizes the dynamic resonant frequency response of the RFQ under various operating conditions including system-level details facilitates the specification of both the water cooling system and the resonant frequency controller, thus reducing design risk and enabling better system optimization.

Simulation of thermal effects in RFQs are often conducted using multi-physics codes such as ANSYS [1, 2, 3 ,4]. These simulations treat the RFQ as a stand-alone system. While this is highly valuable, it is generally too difficult to study both the RFQ thermal response and the full cooling system response in a simulation tool with this level of detail. A simplified thermal capacitance model has been used previously to study system-level effects in RF electron guns [5, 6, 7]. This technique is well suited for cavities with a single water-temperature-to-resonant-frequency relationship; however, RFQs have a water-temperature-to-resonant-frequency relationship that depends on both the vane and the wall temperatures.

The RFQ for the PIP-II Injector Test is currently being commissioned at Fermilab in support of a proposed upgrade to the accelerator complex. This upgrade will increase proton intensity for the next generation of neutrino experiments [8, 9, 10]. In order to understand the frequency transients for our RFQ on a detailed level and over long time scales, we have developed a model that encompasses the temperature and frequency response of the RFQ in conjunction with the thermal response of the cooling system. The thermal response model of the RFQ was an extension of the classical lumped thermal capacitance technique [5, 6, 7]. The temperature-to-frequency coefficients used in this model for the vanes and walls were determined from a set of detailed multi-physics simulations of the RFQ without the dynamics of the external cooling system. These were conducted at LBNL [11].

In this paper we begin with an overview of the water cooling system used for this RFQ, followed by a discussion of our modeling technique. We discuss the model's ability to capture complex thermal relationships in the RFQ. We then demonstrate the performance of the model by comparing temperature and frequency predictions to measured data from the RFQ and water system. These comparisons were done both at low average power (pulsed operation) and at high average power (CW operation), thus demonstrating that this modeling technique can be used to characterize a RFQ water cooling system for both low-power applications and high-power applications.

II. Overview of the RFQ and water system

The RFQ is 4.45 meters long, and is composed of four separate modules connected along the longitudinal axis. It is designed to operate at 162.5 MHz with a nominal RF input power of 100 kW CW. Chilled water is supplied to the RFQ by two parallel loops: one for the inner (vane) channels and one for the outer (wall) channels, as illustrated in Figure 1. The channels are fed via an external cooling circuit, supplied with temperature-regulated water. The ratio of cold water to warm

J. P. Edelen (jedelen@fnal.gov), D. Bowring, B. E. Chase, and J. Steimel are with the Fermi National Accelerator Laboratory, Batavia IL, 60510, USA
A. L. Edelen, S. G. Biedron, and S. V. Milton are with Colorado State University, Fort Collins CO, 80523, USA

Operated by Fermi Research Alliance, LLC under Contract No. DE-AC02-07CH11359 with the United States Department of Energy

This article has been accepted for publication in a future issue of this journal, but has not been fully edited. Content may change prior to final publication. Citation information: DOI 10.1109/TNS.2016.2644663, IEEE Transactions on Nuclear Science

water will later be used to regulate the resonant frequency of the RFQ. Each module of the RFQ has its own water distribution manifold.

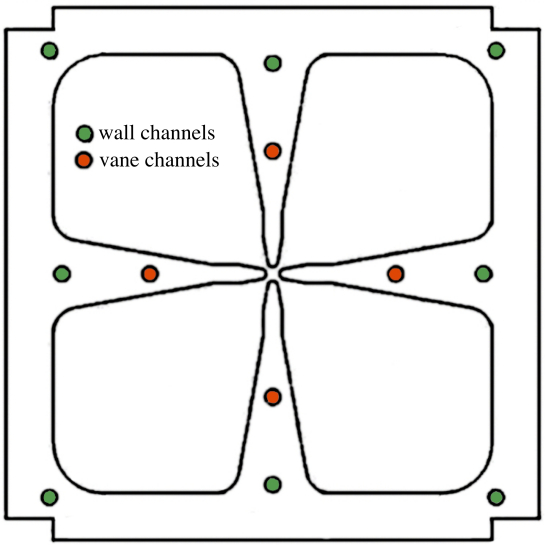

Fig. 1: Cross-section of RFQ showing locations of the vane and wall cooling channels

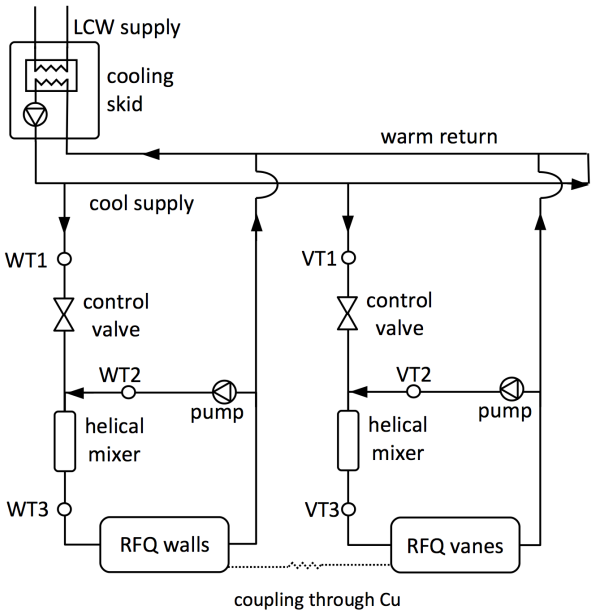

Fig. 2: Block diagram of the water cooling system

The external cooling circuit itself consists of water distribution, two pumps that maintain a constant flow of water into the RFQ, two flow control valves that regulate how much chilled water is mixed into each sub-circuit, and an intermediate skid that regulates the average chilled water supply temperature. The intermediate skid has its own independent temperature control system that maintains the output temperature to within $\pm 0.28°\mathrm{C}$ ($\pm 0.5°\mathrm{F}$). Figure 2 shows a schematic overview of the cooling system. For illustration purposes, we have lumped together the different modules of the RFQ and displayed the water distribution manifolds as a single supply (after VT3 and WT3) and return (before VT2 and WT2) to the RFQ. It is important to note that the system is subject to transport delays for the return water and for the supply water due to the pump and supply lines being located outside the cave. The helical mixers are located just before the distribution manifold to minimize the transport delay between the water mixing point and the RFQ. There are six locations where we have high-resolution temperature sensors suitable for the use in the resonance control system. These sensors are located at the chilled water supply point (WT1 and VT1 for the walls and vanes respectively), on the return line (WT2 and VT2 for the walls and vanes respectively), and after the mixing points (WT3 and VT3 for the walls and vanes respectively). Additionally we have flow and pressure meters throughout the cooling system with high resolution flow meters on the chilled water supply lines.

III. Overview of the Modeling Technique

In order to construct a model that is simple enough for long-timescale simulations (on the order of the characteristic response of the RFQ, 30-40 minutes), but also produces accurate results, we approximate the thermal dynamics in the RFQ, the fluid dynamics of the cooling system, and the geometry of the entire system.

For the cooling system, we begin by approximating each of the water distribution manifolds as two supply and return pipes (i.e. one set for the vane circuit and one set for the wall circuit). This simplifies the transport model and heat transfer model of the cooling system. Additionally, we assume that the transport delays in the plumbing manifold are small compared with the long transport delays associated with the distribution system. We also assume that pumps on the cooling skids completely and perfectly compensate for changes in the chilled supply flow, as designed. In reality, this compensation is not perfect. Finally, we assume that the helical mixers are performing ideal mixing between the chilled water and the return water. For the RFQ, the geometry of the walls and vanes were simplified into two individual thermal capacitances, with a coupling term between them to account for the heat transfer between the walls and vanes. This ignores localized effects on individual sections of the vanes and walls but should capture enough detail to predict temperature and resonant frequency shifts of the RFQ and cooling system with reasonable accuracy. Estimates of the parameters in this model are described in Section IV.

A. Thermal response of the RFQ

The thermal model of the RFQ begins with the classical lumped capacitance [5] for an RF cavity

$$\begin{aligned} T_{\mathrm{out}}(t) =& T_{\mathrm{initial}} + \frac{1}{C}\int_0^t P_{\mathrm{rf}}(t)dt \\ & - \frac{1}{C}\int_0^t \left(\frac{(T_{\mathrm{out}}(t) - T_{\mathrm{in}}(t))\dot{V}}{A}\right) dt. \end{aligned} \tag{1}$$

This article has been accepted for publication in a future issue of this journal, but has not been fully edited. Content may change prior to final publication. Citation information: DOI 10.1109/TNS.2016.2644663, IEEE Transactions on Nuclear Science

Here, $T_{\mathrm{out}}(t)$ is the temperature of the water leaving the cavity. We assume that the temperature of the water leaving the cavity is approximately equal to the temperature of the cavity [ibid]. C is the thermal capacitance [J/°C] of the cavity, $P_{\mathrm{rf}}(t)$ is the RF heating, $T_{\mathrm{in}}(t)$ is the temperature of the water at the input to the cavity cooling channel, $\dot{V}$ is the volume flow rate of the water in the cavity, and A is the heat carrying capacity of water. We model the time-dependent temperature of the walls and vanes in the RFQ using Equation 1, with a coupling term that accounts for heat transfer between the two subsystems through the copper. We also add a term to account for thermal losses to the environment from the walls. Equations 2 and 3 show the thermal models for the vanes and walls respectively.

$$\begin{aligned} T^{\mathrm{v}}_{\mathrm{out}}(t) =& T^{\mathrm{v}}_{\mathrm{initial}} + \frac{1}{C^{\mathrm{v}}}\int_0^t P^{\mathrm{v}}_{rf}(t)dt \\ &- \frac{1}{C^{\mathrm{v}}}\int_0^t \left(T^{\mathrm{v}}_{\mathrm{out}}(t) - T^{\mathrm{w}}_{\mathrm{out}}(t)\right) K_1 dt \\ &- \frac{1}{C^{\mathrm{v}}}\int_0^t \left(\frac{(T^{\mathrm{v}}_{\mathrm{out}}(t) - T^{\mathrm{v}}_{\mathrm{in}}(t))\dot{V^{\mathrm{v}}}}{A}\right) dt \end{aligned} \tag{2}$$

Here $T^{\mathrm{v}}_{\mathrm{out}}$ is the temperature of the water at the output of the vane channels, C^{v} is the thermal capacitance of the vanes, P^{v}_{rf} is the RF power heating the vanes, $T^{\mathrm{v}}_{\mathrm{in}}$ is the input temperature to the vane cooling channels, $T^{\mathrm{w}}_{\mathrm{in}}$ is the input temperature to the wall cooling channels (this is used to account for the coupling between the vane and wall circuits through the copper), K_1 is a coefficient that describes the coupling between the two circuits through copper, $\dot{V^{\mathrm{v}}}$ is the volume flow rate of the water in the vane cooling channels, A is the heat carrying capacity of water, and $T^{\mathrm{v}}_{\mathrm{initial}}$ is the initial temperature of the vanes at the start of the simulation.

$$\begin{aligned} T^{\mathrm{w}}_{\mathrm{out}}(t) =& T^{\mathrm{w}}_{\mathrm{initial}} + \frac{1}{C^{\mathrm{w}}}\int_0^t P^{\mathrm{w}}_{\mathrm{rf}}(t)dt \\ &- \frac{1}{C^{\mathrm{w}}}\int_0^t \left(T^{\mathrm{w}}_{\mathrm{out}}(t) - T^{\mathrm{v}}_{\mathrm{out}}(t)\right) K_1 dt \\ &- \frac{1}{C^{\mathrm{w}}}\int_0^t \left[\frac{(T^{\mathrm{w}}_{\mathrm{out}}(t) - T^{\mathrm{w}}_{\mathrm{in}}(t))\dot{V^{\mathrm{w}}}}{A}\right] dt \\ &- \frac{1}{C^{\mathrm{w}}}\int_0^t \left(T_{\mathrm{air}}(t) - T^{\mathrm{w}}_{\mathrm{out}}(t)\right) K_2 dt. \end{aligned} \tag{3}$$

In Equation 3, many of the terms are the same as Equation 2 but cast from the perspective of the wall circuit. Additionally, the last term describes the heat transfer between the RFQ walls and the environment via the coefficient K_2. This is only included for the wall component because the vanes are not in direct contact with the atmosphere. T_{air} is the air temperature.

Using Equations 2 and 3, we can calculate the resonant frequency shift of the RFQ

$$\begin{aligned} \Delta f_0(t) = (T^{\mathrm{w}}_{\mathrm{out}}(t) - T^{\mathrm{w}}_{\mathrm{initial}})\frac{\Delta f_0}{\Delta T^{\mathrm{w}}} \\ +(T^{\mathrm{v}}_{\mathrm{out}}(t) - T^{\mathrm{v}}_{\mathrm{initial}})\frac{\Delta f_0}{\Delta T^{\mathrm{v}}}. \end{aligned} \tag{4}$$

Here $\frac{\Delta f_0}{\Delta T^{\mathrm{w}}}$ is the frequency shift per °C change in the wall temperature, and $\frac{\Delta f_0}{\Delta T^{\mathrm{v}}}$ is the frequency shift per °C change in the vane temperature. From Equations 2-4, we have a simple thermal model for the RFQ that can be combined with models for the water transport and mixing to study system-level behavior.

B. Heating due to friction

There is heating of the water that occurs throughout the system due to friction. This heating takes place where pressure drops occur in the plumbing. For this model we have combined these into a single heating term applied at the pump. This heating is approximated using Equation 5.

$$\Delta T = \frac{P_{\mathrm{pump}}}{c_{\mathrm{water}}\dot{m}} \tag{5}$$

Here, ΔT is the temperature change of the water due to frictional heating, P_{pump} is the pump power, c_{water} is the specific heat of water, and $\dot{m}$ is the mass flow rate of water through the pump. The pump power is calculated using the pressure drop across the pump multiplied by the flow rate of the water through the pump.

C. Heat transfer in the pipes

Heat transfer from the pipes to the atmosphere is modeled as a temperature change over a length of straight pipe for some given external temperature, as shown in Equation 6:

$$T_{\mathrm{out}}(t-t_d) = T_{\mathrm{air}}(t) - (T_{\mathrm{air}}(t) - T_{\mathrm{in}}(t))\exp\left(\frac{-k'L}{r_{\mathrm{i}}^2 c\rho v}\right). \tag{6}$$

Here T_{out} is the temperature of water after traversing the length of pipe, T_{air} is the air temperature, T_{in} is the temperature of water entering the section of pipe, k' is the effective thermal conductivity, h is the convective heat transfer coefficient of stagnant air, (approximately 10-25 W/m^2 K, we used 17 W/m^{2}K), L is the length of the pipe, r_i is the inner radius of the pipe, r_0 is the outer radius of the pipe, c is the specific heat of water, ρ is the density of water at room temperature, and v is the velocity of water in the pipe. The effective thermal conductivity is given by $k' = kr'\left(2hr_0/(2hr_0 + kr')\right)$, where r' is the effective pipe thickness, $r' = (r_0 + r_{\mathrm{i}})/(r_0 - r_{\mathrm{i}})$. The time delay t_{d} of the transport section is calculated using the volume flow rate and the pipe area, with the assumption that the velocity of the water in the pipe is constant.

D. Mixing

We assume ideal mixing of the cold and warm water, given by Equation 7. Because we have helical mixers specifically designed to provide close to ideal mixing, this is a reasonable approximation.

$$T_{\mathrm{out}} = \frac{T_1\dot{V}_1 + T_2\dot{V}_2}{\dot{V}_1 + \dot{V}_2} \tag{7}$$

T_1 and T_2 are the two input temperatures, and $\dot{V}_1$ and $\dot{V}_2$ are the two input volume flow rates.

This article has been accepted for publication in a future issue of this journal, but has not been fully edited. Content may change prior to final publication. Citation information: DOI 10.1109/TNS.2016.2644663, IEEE Transactions on Nuclear Science

IV. Modeling the RFQ cooling system

Using the equations in Section III we constructed a model of the RFQ and water system using Matlab's Simulink simulation framework [12]. Figure 3 shows a block diagram of the model. Note that a superscript w or v denotes the wall or vane circuit respectively. Each block represents a system component that is modeled in Simulink. Using the inputs at each time-step, the simulation calculates the water temperature at each location in the cooling system. The thermal model of the RFQ is used to calculate frequency shifts using Equation 4.

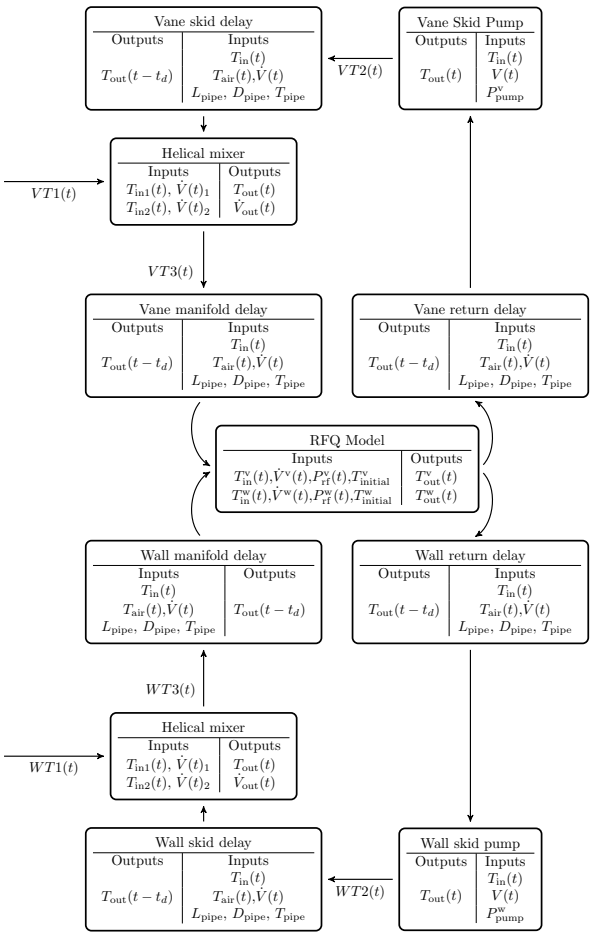

Fig. 3: Block diagram of the water system model

Here $T_{\rm out}(t-t_d)$ is the temperature of the water leaving a block (note that in the pipe transport sections the output temperature is delayed by $t_{\rm d}$), $T_{\rm in}(t)$ is the temperature of water at the input to a block, $T_{\rm air}(t)$ is the ambient air temperature, $\dot{V}(t)$ is the volume flow rate of water entering the block, $P_{\rm rf}$ is the effective RF heating for either the walls or vanes, $T_{\rm initial}$ is the initial temperature of the RFQ, $L_{\rm pipe}$ is the length of pipe for a transport section, $D_{\rm pipe}$ is the outer diameter of the pipe for a transport section, $T_{\rm pipe}$ is the pipe thickness for a transport section, and $P_{\rm pump}$ is the power of the pump. The system parameters used for the model are given by Table 1.

The thermal capacitances for the vane and wall circuits were determined by estimating the mass of the vanes and walls using the machining drawings for the RFQ. The pump heating powers were calculated from the nominal pressure drop and volume flow rate through the pumps. The frequency shift coefficients were obtained from 2-D ANSYS results [11]. The heat transfer coefficient K_1 between the vane and walls was estimated using a 1-D heat transfer model between the vane cooling channel and the nearest wall cooling channel (in doing so we assume that most of the heat transfer occurs between each vane cooling channel and the nearest wall cooling channel). Equation 8 gives the conductive heat transfer equation.

TABLE I: Model parameters for our RFQ

Model parameter	Estimate	Units
$C^{\rm v}$	160	kJ/°C
$C^{\rm w}$	1430	kJ/°C
K_1	0.943	kW/°C
K_2	0.073	kW/°C
$P^{\rm w}_{\rm pump}$	2.9	kW
$P^{\rm v}_{\rm pump}$	1.6	kW
$\Delta f_0/\Delta T^{\rm w}$	13.9	kHz/°C
$\Delta f_0/\Delta T^{\rm v}$	-16.4	kHz/°C
Vane total flow	89	GPM
Wall total flow	167	GPM

$$Q_{\rm cond} = \frac{k_{\rm cu} A \Delta T}{d} \tag{8}$$

Here $k_{\rm cu}$ is the thermal conductivity of copper [398 W / m·K], A is the heat transfer area [m^2], estimated using the area of the walls in direct contact with the vanes, (~ 0.192 m^2 over the whole RFQ), and d is the distance between the vane and wall cooling channels, ($\sim$ 0.081 m). This gives a coupling coefficient of 943 W/ °C.

The coupling coefficient between the RFQ and the environment, K_2, is computed through the use of Equations 9, 10, and 11 which represent the conductive, radiative, and convective heat transfer rates respectively. For these calculations the surface area for the RFQ was estimated using the bulk RFQ dimensions obtained from mechanical drawings, giving $A \approx 9$ m^2.

$$Q_{\rm cond} = \frac{kA\Delta T}{d} \tag{9}$$

For the conductive heat transfer coefficient, $Q_{\rm cond}$, k is the thermal conductivity of air ($\sim 26.3 \times 10^{-3}$ W/m·°C), ΔT is the temperature differential between the RFQ and the air in the building, and d is the effective distance for conduction (≈ 1 m). This gives a heat transfer coefficient for conductive losses of ~ 2.38 W/°C.

$$Q_{\rm rad} = A\epsilon\sigma(T^4 - T^4_{\rm ambient}) \tag{10}$$

For the radiative heat transfer coefficient $Q_{\rm rad}$, ϵ is the emissivity (estimated at 0.78 due to oxidation [13], and σ is the Stefaan-Boltzmann constant. This gives a heat transfer coefficient of $\sim$ 443 W when the RFQ is at 35 °C and the

This article has been accepted for publication in a future issue of this journal, but has not been fully edited. Content may change prior to final publication. Citation information: DOI 10.1109/TNS.2016.2644663, IEEE Transactions on Nuclear Science

ambient temperature is at 25 °C. Because $(T^4 - T^4_{\text{ambient}})$ is approximately linear over the relatively small changes in temperature (± 10°C), we approximated the radiative heat transfer coefficient as 44.3 W/°C. While this approximation is not necessary for such a simple calculation, it significantly reduces the complexity of the interconnections in Simulink.

$$Q_{\text{conv}} = h_c A \Delta T \tag{11}$$

For the convective heat transfer rate between the RFQ and the atmosphere, Q_{conv}, we need to treat the four different surfaces of the RFQ separately in order to account for their different convection coefficients. The convection coefficient can be described by $h = \text{Nu}_\text{L} k/L$, where Nu_L is the Nusselt number, k is the thermal conductivity of air, and L is the effective length of convection. As the Nusselt number varies significantly for hot surfaces facing upward vs. hot surfaces facing downward, approximate values for different scenarios given by [13] were used to determine our estimates. Given the approximate Nusselt numbers, the convective heat transfer coefficient for the upper surface and the lower surface are estimated as $h_\text{t} = 4.2$ and $h_\text{b} = 1.56$ respectively. For the two sides of the RFQ the convection coefficient was estimated to be $h = 2.97$. Adding the different convective heat transfer rates for the RFQ gives a net heat transfer coefficient between the RFQ and the atmosphere due to convection of $\sim$ 26.4 W/°C. Adding each of the heat transfer coefficients derived from Equations 9, 10, and 11, gives a total estimated coupling coefficient between the RFQ and the environment of $\sim$ 73 W/°C.

V. Low-power validation

During low-power testing we studied the temperature and frequency response of the RFQ and water system in three stages of increasing complexity. First, only two RF power levels were examined with no changes in the flow control valve settings. Second, two RF power levels with 20 combinations of wall and vane flow valve settings were examined. Third, six RF power levels with five combinations of flow valve settings were examined. Throughout these studies the RF system was operating in pulsed mode with a pulse length of 4 ms at a 10 Hz repetition rate. RF parameters, chilled water flow, ambient temperature, and water temperature data throughout the system were collected at a 1Hz rate. For each of the studies we compute the root mean squared (RMS) error between the simulation and measurements, maximum error between the simulation and measurements, the peak-to-peak temperature change during the study, and the ratio of the RMS error to the temperature range. Figures 4 and 5 show the inputs to the model and the comparison of the model to the measurements for the third test. This test had changes in both the RF heating as well as the flow control valves.

Figure 4a shows the range of total RF power used for this comparison. Fast drops in the RF power were trips caused by reflected power. Figure 4b shows the change in the flow due to the flow control valve. Note that there is a correlated change in the wall valve from a change in the vane valve; this is caused by coupling in the intermediate skid loop shown in Figure 2. Figure 4c shows the fluctuation in the cave temperature as well as the chilled supply temperature during this study. Note that while the supply temperature is not actively being changed the regulation loop on the intermediate skid does not completely remove fluctuations in the supply temperature.

The inputs to the model for this study include the RF power settings, the chilled water flow settings, and the ambient and supply temperatures. As noted in Section II, the temperatures of the water going into the RFQ are WT3 and VT3 for the wall and vane circuit respectively, and the return temperatures measured at the skid are WT2 and VT2 for the wall and vane circuits respectively.

In Figure 5 we see a correlated increase in the error as a function of time. This is due to discrepancies between the model and the measurements in predicting changes due to the flow valve. Generally speaking though, the model and the measurements agree quite well. Tables 2 through 4 show the RMS error, peak error, temperature range, and ratio of the RMS error to the temperature range for all three studies.

TABLE II: RMS error, max error, temperature range during the test, and the ratio of the RMS error to the temperature range during the first case study

Sensor	RMS Error	Max. Error	Range	RMS/Range
WT2	0.10 [°C]	0.16 [°C]	1.20 [°C]	0.08
WT3	0.03 [°C]	0.09 [°C]	1.15 [°C]	0.03
VT2	0.15 [°C]	0.42 [°C]	1.07 [°C]	0.14
VT3	0.32 [°C]	0.53 [°C]	1.01 [°C]	0.32

TABLE III: RMS error, max error, temperature range during the test, and the ratio of the RMS error to the temperature range during the second case study

Sensor	RMS Error	Max. Error	Range	RMS/Range
WT2	0.17 [°C]	0.46 [°C]	1.94 [°C]	0.09
WT3	0.22 [°C]	0.54 [°C]	1.90 [°C]	0.12
VT2	0.16 [°C]	0.39 [°C]	2.20 [°C]	0.07
VT3	0.31 [°C]	0.58 [°C]	2.21 [°C]	0.14

TABLE IV: RMS error, max error, temperature range during the test, and the ratio of the RMS error to the temperature range during the third case study

Sensor	RMS Error	Max. Error	Range	RMS/Range
WT2	0.13 [°C]	0.31 [°C]	1.51 [°C]	0.09
WT3	0.18 [°C]	0.36 [°C]	1.47 [°C]	0.12
VT2	0.22 [°C]	0.73 [°C]	1.65 [°C]	0.13
VT3	0.28 [°C]	0.76 [°C]	1.64 [°C]	0.17

Tables 2, 3, and 4 show that under a wide variety of conditions the model can accurately predict the temperature changes in the cooling loops. The RMS error in all cases was below 0.32 °C. Additionally, for all studies the ratio of the RMS error to the temperature range was below 0.17. Of the four temperature sensors, the prediction at VT3 consistently performs worse than that at the other sensors and is consistently underestimated in the simulation. This is due to a known calibration issue in the sensor giving a DC offset to the data that is not captured by our model. The standard deviation of the error however, is less than or equal to 0.15 °C across all data sets. This indicates that relative changes in temperature

This article has been accepted for publication in a future issue of this journal, but has not been fully edited. Content may change prior to final publication. Citation information: DOI 10.1109/TNS.2016.2644663, IEEE Transactions on Nuclear Science

are predicted with a higher degree of accuracy than absolute temperatures. Tables V and VI show the standard deviation of the error and the ratio of the standard deviation of the error to the temperature range for all four sensors across all three tests.

TABLE V: Standard deviation of the error, for each temperature sensor across all three tests

Sensor	Test 1	Test 2	Test 3
WT2	0.030 [°C]	0.15 [°C]	0.12 [°C]
WT3	0.029 [°C]	0.15 [°C]	0.12 [°C]
VT2	0.11 [°C]	0.11 [°C]	0.15 [°C]
VT3	0.094 [°C]	0.095 [°C]	0.13 [°C]

TABLE VI: Ratio of the standard deviation of the error to the temperature range, for each temperature sensor across all three tests

Sensor	Test 1	Test 2	Test 3
WT2	0.025	0.079	0.082
WT3	0.026	0.078	0.081
VT2	0.10	0.050	0.088
VT3	0.093	0.043	0.082

While Tables II - IV show that in general we can use this model for studying absolute temperature transients at the system level within 20%, Table VI suggests that we can predict relative changes to within 10%.

Next we compare the predicted changes in resonant frequency to measurements of the resonant frequency derived from the forward-to-cavity phase measured using the RF signals. Equation 12 gives the shift in the resonant frequency as a function of the measured forward phase and the cavity phase.

$$\delta f_0 = \frac{\tan\left(\phi_{\mathrm{cav}} - \phi_{\mathrm{fwd}}\right)}{2Q_{\mathrm{L}}} f_0 \tag{12}$$

Here, f_0 is the drive frequency, ϕ_{fwd} is the forward phase, ϕ_{cav} is the cavity phase, Q_{L} is the loaded quality factor, and δf_0 is the shift in resonant frequency. For these studies the drive frequency was 162.465 MHz, and Q_{L} was 6900. Because our RFQ is driven by two amplifiers, the forward phase is determined by taking the vector sum of the two drive signals at the input to the cavity. Figure 6 shows the comparison between the model and the measurements of resonant frequency changes during the test illustrated in Figures 4 and 5.

Here we see relatively good agreement between the simulations and the measurements, and as with the temperature predictions there is a steady increase in the error with time. Table VII shows the RMS, peak error, frequency range, and the ratio between the RMS error and the frequency range for tests two and three. Test 1 was omitted because of the large number of RF trips resulting in a poor comparison due to the lack of data on the RFQ frequency.

This section shows good agreement between the model and measurements for low power operation. We have shown that in general the model can predict changes in frequency or temperature to better than 15% over a wide range of operational conditions. In order to confirm that the model will still provide meaningful predictions at high power we compared measurements with predictions during the first CW run.

TABLE VII: RMS error, max error, frequency range during the test, and the ratio of the RMS error to the frequency range for Figures 20 and 21

Test	RMS Error	Max. Error	Range	RMS/Range
Test 2	2.9 [kHz]	7.04 [kHz]	19.16 [kHz]	0.15
Test 3	1.67 [kHz]	4.01 [kHz]	12.02 [kHz]	0.14

VI. High-power validation

During high-power testing we studied the temperature and frequency response of the RFQ and water system in three stages of increasing complexity similar to the low-power validation in Section IV. Additionally one of the goals for the first CW run was to bring the RFQ up to full power and tune to its design frequency and engage LLRF feedback. Because this required adjustments to the supply temperature and the flow control valves, the test serves as a fairly good representation of normal operating conditions. Additionally in order to run CW at the desired frequency we needed to decrease the supply temperature to 20 °C. At this temperature the design frequency is approximately +50 kHz at full power. The cooling power for the walls and vanes at the nominal flow rates is approximately 57 kW and 23 kW respectively. The cooling to air is approximately 1 kW. Figure 7 shows the ambient cave temperature, vane supply temperature, and wall supply temperature during the test.

The initial RF load on the cooling system caused the building chiller to trip at 1.5 hours into testing. After reset, operation was stable during the rest of testing. During the time of the chiller trip, RF was turned off. After reseting this, the temperature returned to the nominal set-point of 20 °C. The saw-tooth fluctuations in the chilled supply temperature are due to the intermediate skid's independent control system. During this study we were mostly controlling the vane valve to maintain the resonant frequency, with some minor adjustments to the wall valves.

Using the data shown in Figure 7, we predicted the temperatures in the cooling system at the supply to the RFQ (VT3 and WT3 for the vanes and walls respectively) and at the return by the skid (VT2 and WT2 for the vanes and walls respectively). Figure 8 shows the comparison of the model to the measurements for these four temperature sensors.

Here we see good agreement between the simulated temperatures and the measured temperatures for all four sensors, comparable to the agreement shown during pulsed operation in Section VI. Figure 9 shows the measured frequency shift throughout the test compared with the simulated frequency shift.

There are a few times during the test where where we lost RF power (as seen in Figure 7). This results in a loss of the cavity frequency measurement for some period of time. For comparison purposes we chose to hold the last measured frequency value during the region where there is no measurement available. Figure 9 shows that in general the

model is adequately predicting the frequency response of the RFQ. It does appear to consistently over-predict fast transients in the RFQ frequency. This is likely due to inaccuracies in one or more of the parameters used to construct the model. In Section VII we address the sensitivity of the model to perturbations in the parameters.

TABLE VIII: RMS error, maximum error, frequency range during the test, and the ratio of the RMS error to the frequency range for CW Testing

	RMS Error	Max. Error	Range	RMS/Range
WT2	0.63 [°C]	1.52 [°C]	10.95 [°C]	0.06
WT3	0.71 [°C]	1.81 [°C]	10.27 [°C]	0.07
VT2	1.49 [°C]	4.29 [°C]	9.92 [°C]	0.15
VT3	0.77 [°C]	2.94 [°C]	9.04 [°C]	0.08
Frequency	12.63 [kHz]	52.77 [kHz]	100.00 [kHz]	0.13

Table 8 shows that in general the model predicts measurements to better then 15%. This demonstrates that the modeling technique used to evaluate RFQ temperature and frequency shifts when operating with low average power (pulsed RF) can be extended to high average power operation (CW RF).

VII. Model sensitivity analysis

Sections V and VI show that we can predict changes in the frequency and temperature to within 11% on average. However the parameters used in the model rely on significant approximations described in Section III. In order to understand which parameters most affect the model predictions, we calculated the derivative of the ratio of the RMS error to the range with respect to a change in each of the parameters shown in Table 1. Figures 10 and 11 show the sensitivity of the error to each of the parameters in Table 1 for pulsed and CW operation respectively.

Here we see that in general the model is most sensitive to perturbations in the coupling coefficients, and the model is very insensitive to changes in the thermal mass and the flow rates. It is also interesting that the model is not very sensitive to the frequency coefficients for the vanes and walls. Thus, in the current configuration, errors in the coupling coefficients are expected to dominate the overall modeling error

VIII. Conclusions

In this paper, we have shown that our a priori model can efficiently predict changes in the temperature and resonant frequency to within 11% on average while including the system-level effects in the cooling system. Additionally we have shown that the model can predict relative changes in temperature to within 7% on average. While high-fidelity multiphysics modeling software is often used to simulate the thermal behavior of individual elements in such a system (most typically the cavity itself), such modeling is often too computationally expensive to be effective when studying large, distributed systems with many interdependent components, including pumps, valves, and controllers. The ability to study temperature and frequency shifts at the system level with a reasonable degree of accuracy is paramount to the design, simulation, and optimization of control algorithms for maintaining the resonant frequency of an RFQ, as well as guiding hardware design (e.g. the cooling system).

Prior to the delivery of the RFQ and obtaining the validation results described above, this model was used to aid in the design of the water cooling system for the PIP-II Injector Test RFQ. Now that it has been validated, it can be used as a design tool for future high power RFQs, their cooling systems, and their proposed controllers prior to installation. This technique could be extended using gathered data on a system to fit some of the estimated coefficients, resulting in a more accurate representation of the system dynamics.

IX. Acknowledgements

The authors would like to thank Maurice Ball and Jerzy Czajkowski for leading the water system design and debugging, and for many fruitful discussions. Thanks also to Tom Zuchnik and Dennis Nicklaus, who were instrumental in the data acquisition design, installation, and debugging. The authors would also like to thank Ed Cullerton for his work on the LLRF system, and Curtis Baffes for his many contributions as the lead mechanical engineer for the PIP-II Injector Test. Operated by Fermi Research Alliance, LLC under Contract No. De-AC02-07CH11359 with the United States Department of Energy

References

[1] S. Virostek, M. Hoff, A. Lambert, D. Li, and J. Staples, G. Romanov, and C. Zhang, *Design and analysis of the PXIE CW Radio-Frequency Quadrupole (RFQ)* Pceedings of IPAC2012, New Orleans, Louisiana, USA

[2] S. Virostek, J. Staples, *Analysis of thermally induced frequency shift for the spallation neutron source RFQ* LINAC 2000, eConf C000821 (2000) THD04

[3] Y. Kondo, K. Hasegawa, T. Morishita, H. Matsumoto, F. Naito, *Thermal characteristics of a new RFQ for J-PARC*, IPAC 2010

[4] Y. Kondo et al, *High-power test and thermal characteristics of a new radio-frequency quadrupole cavity for the Japan Proton Accelerator Research Complex linac* PRST-AB 16, 040102 (2013)

[5] J. Crisp, and J. Satti, *Fermilab linac upgrade side coupled cavity temperature control system* IEEE 0-7803-0135-8/91

[6] J. Crisp , and J Satti *Temperature (or Frequency) control system* Fermilab internal report

[7] J. Crisp, *LINAC temperature loops* Fermilab internal report

[8] V. Lebedev Editor, *The PIP-II Reference Design Report* June 2015

[9] *Functional Requirements Specification - PXIE* Feb 2013

[10] D. Bowring, B. Chase, J. Czajkowski, J. Edelen, D. Nicklaus, J. Steimel, T. Zuchnik, A. Edelen, S. Biedron, S. Milton, *Resonance control for Fermilab's PXIE RFQ*, Proceedings of the 2016 International Particle Accelerator Conference, Busan, Korea, 8 - 13 May 2016

[11] A. Lambert's *FNAL PXIE - 162.5 MHZ RFQ GENERAL RF, Thermal, Mechanical, RF Finite Element Analysis*, LBNL Engineering Note 10773, 11 Jan 2013

[12] MATLAB and Statistics Toolbox Release 2016a, The MathWorks, Inc., Natick, Massachusetts, United States.

[13] Moran, Shapiro, Munson, Dewitt *Introduction to Thermal Systems Engineering*

This article has been accepted for publication in a future issue of this journal, but has not been fully edited. Content may change prior to final publication. Citation information: DOI 10.1109/TNS.2016.2644663, IEEE Transactions on Nuclear Science

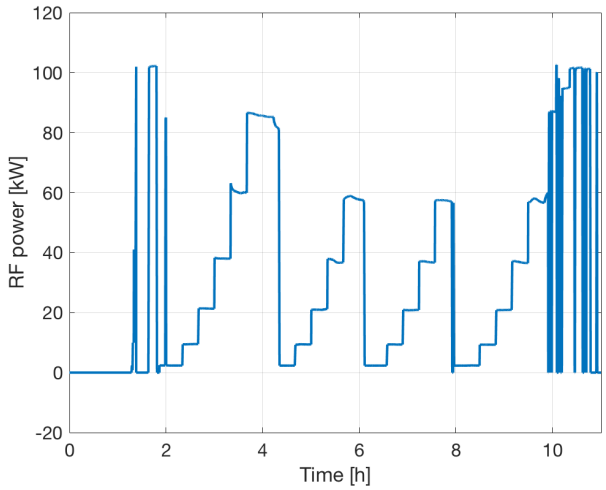

(a) RF power as a function of time throughout test 3

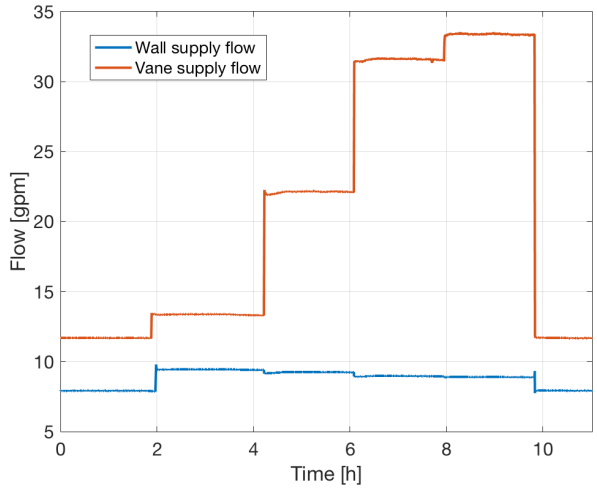

(b) Chilled water flow (measured at VT1 and WT1 for the vanes and walls respectively) as a function of time throughout test 3

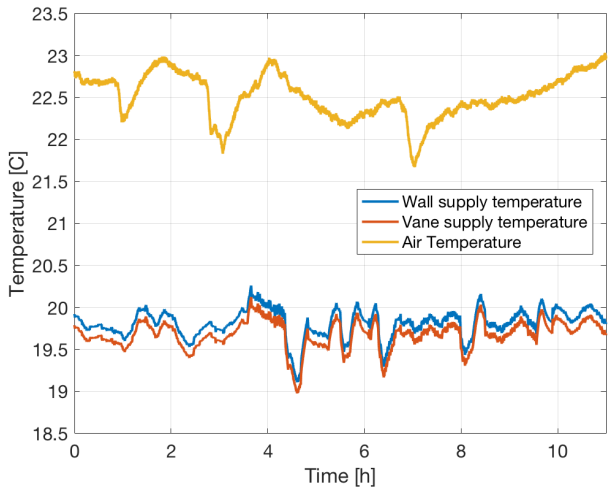

(c) Variation in the chilled water supply temperature (VT1 for the vanes and WT1 for the walls) and the ambient temperature during test 3

Fig. 4: Inputs to the model for the third case study; both the RF amplitude and the flow valves were scanned

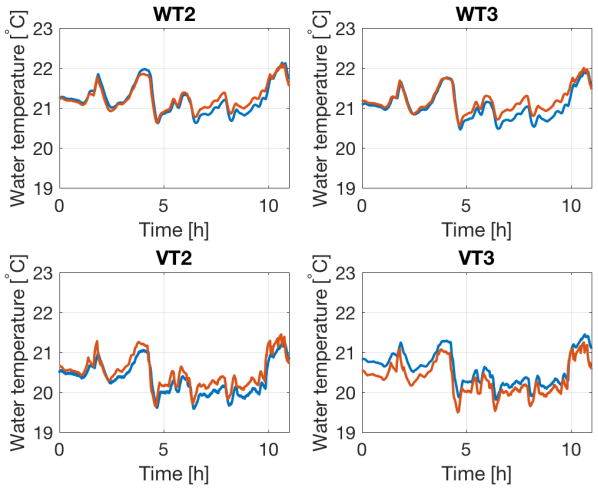

(a) Comparison of measurement (blue) to simulation (red) for test 3

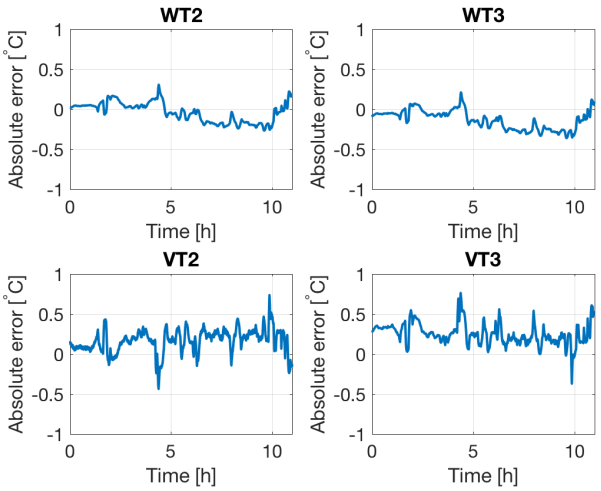

(b) Absolute error between measurement and simulation for test 3

Fig. 5: Comparison between measurement and simulation for the second case study; both the RF amplitude and the flow valves were scanned

This article has been accepted for publication in a future issue of this journal, but has not been fully edited. Content may change prior to final publication. Citation information: DOI 10.1109/TNS.2016.2644663, IEEE Transactions on Nuclear Science

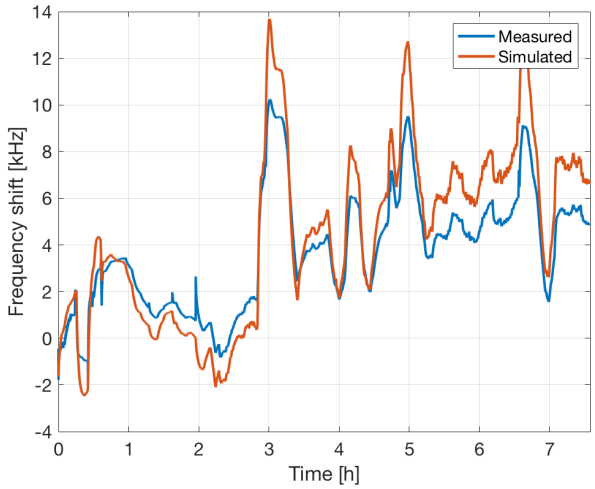

Fig. 6: Comparison of measured frequency shift to simulation for test 3 where both the RF amplitude and the flow valves were scanned

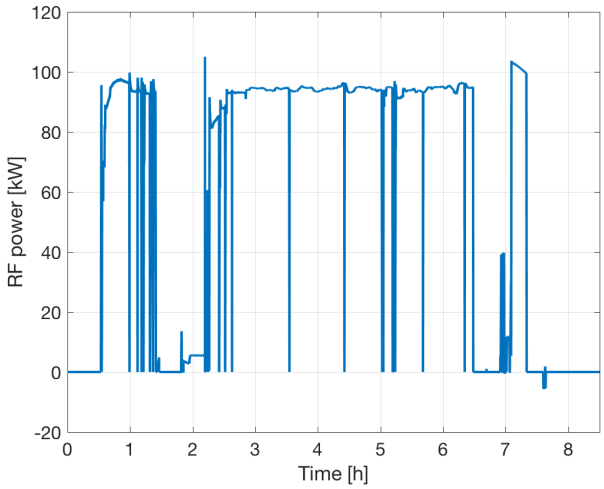

(a) RF power during the study. Note that at hour 7 we switched back to pulsed operation briefly

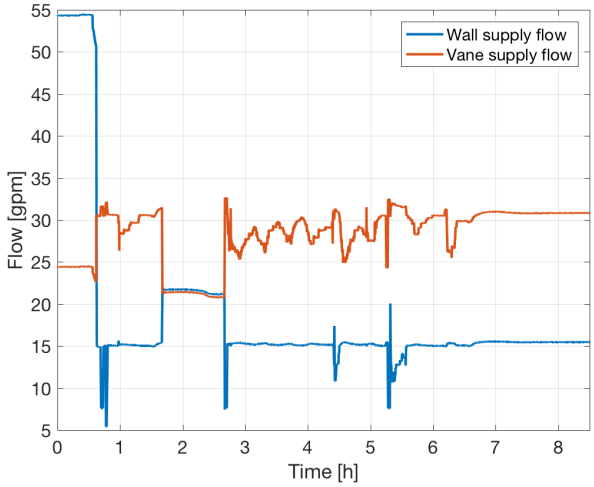

(b) Chilled water (VT1 and WT1 for the vanes and walls respectively) flow during the testing

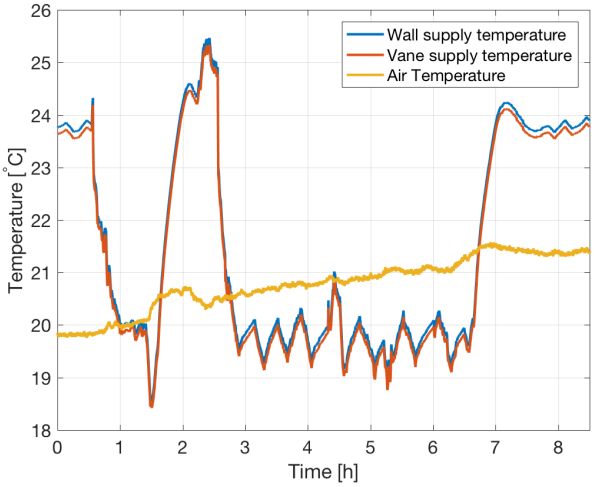

(c) Supply temperature (VT1 for the vanes and WT1 for the walls) and air temperature during the CW studies

Fig. 7: Inputs to the model for the third case study; both the RF amplitude and the flow valves were scanned

This article has been accepted for publication in a future issue of this journal, but has not been fully edited. Content may change prior to final publication. Citation information: DOI 10.1109/TNS.2016.2644663, IEEE Transactions on Nuclear Science

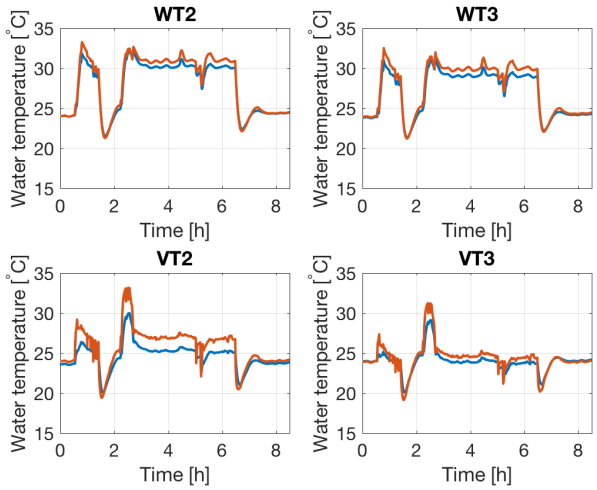

(a) Comparison of model (red) to measurements (blue) during CW operation for four temperature sensors in the cooling system

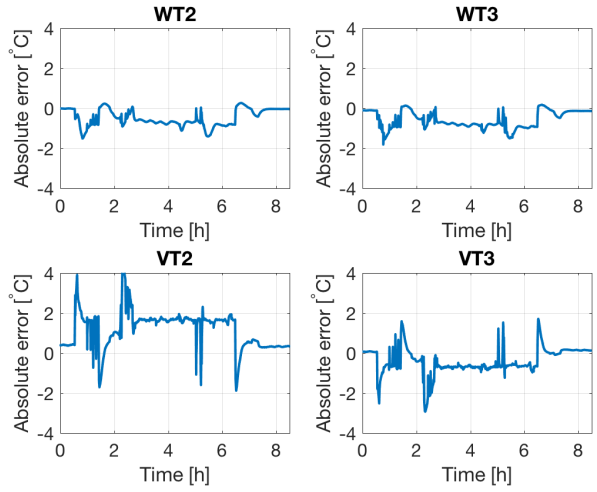

(b) Error between measurement and simulation

Fig. 8: Comparison of measured frequency shift to simulated frequency shift for studies with RF heating

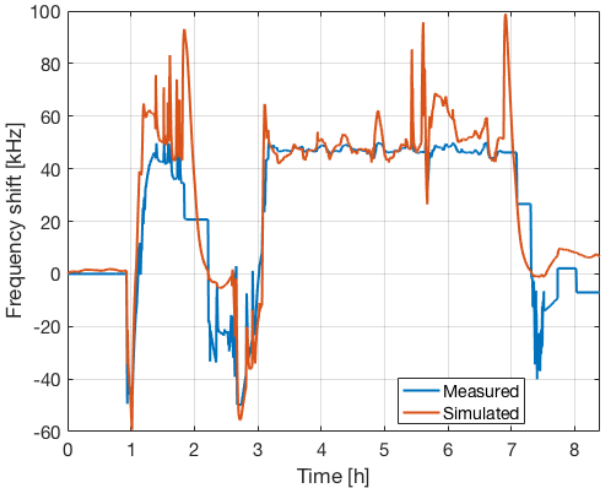

Fig. 9: Comparison of measurements to simulations for the frequency shift in the RFQ during CW testing

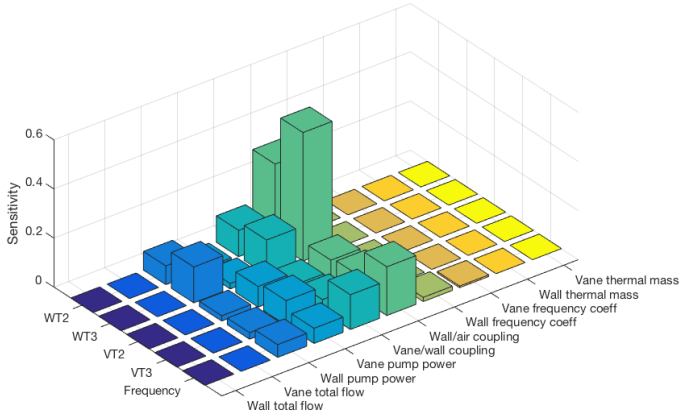

Fig. 10: Absolute sensitivity of the model to 20% perturbation in the parameter during pulsed operation

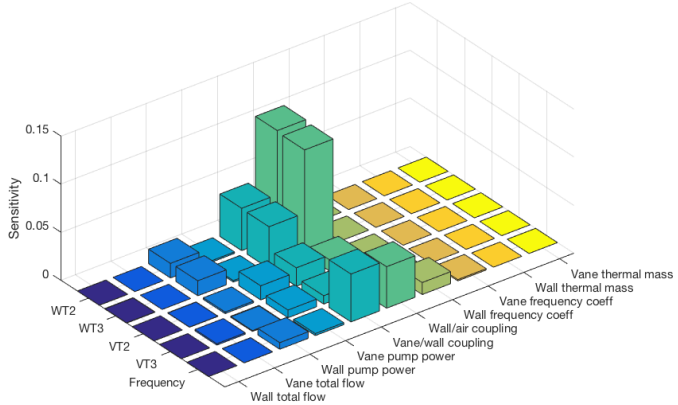

Fig. 11: Absolute sensitivity of the model to 20% perturbation in the parameter during CW operation